

# On residual $^{137}\text{Cs}$ on shallow rugged reefs lying inshore of Fukushima: Part 1: Levels, distribution, and flux of radiations

Fumie Suzuki<sup>\*1</sup>, Hideo Ohashi<sup>1</sup>, Ken-ichi Nogami<sup>1</sup>, Hiromi Shibata<sup>1,3</sup>, Hisayuki Arakawa<sup>2</sup>, Kentaro Umeda<sup>4</sup>, Teiji Kobayasi<sup>5</sup>, and Nobuhiro Shiotani<sup>1</sup>

<sup>1</sup>EcoStudies Association, Toranomon 2-2-5, Minato, Tokyo 105-0001, Japan

<sup>2</sup>Faculty of Marine Resources and Environment, Tokyo University of Marine Science and Technology, Minato, Tokyo 108-8477, Japan

<sup>3</sup>SANKEN (The Institute of Scientific and Industrial Research), Osaka University, Ibaraki, Osaka 567-0047, Japan

<sup>4</sup>Department of Electric and Electronic Engineering, Tohoku Institute of Technology, Yagiyama-Kasumichou, 35-1, Sendai 982-8577, Japan

<sup>5</sup>Emeritus Prof. of Tohoku University, Choumei-ga-Oka, 4-26-8, Sendai 981-3212, Japan

\*Corresponding author: Fumie Suzuki.

e-mail address: [suzuki@ecostudies.jp](mailto:suzuki@ecostudies.jp)

## Abstract

Levels of residual  $^{137}\text{Cs}$  on reefs lying inshore of Fukushima were measured with the use of a newly improved underwater CsI(Tl) gamma-ray spectrometer. The levels varied from point to point, ranging from  $1.0 \times 10^4$  Bq/m<sup>2</sup> to  $9.9 \times 10^4$  Bq/m<sup>2</sup>. All the measured spectra showed the presence of significant amounts of flux of gamma rays of energies less than 662 keV. With the use of an empirically determined spectrum of the Compton continuum inevitably created in the detector, a true spectrum of low energy gamma rays on and near the interface between contaminated rock surface and seawater was obtained. Analyses of transport of 662 keV gamma rays confirmed that those low energy gamma rays were derived from the multiple Compton scattering of 662 keV gamma rays emitted from residual  $^{137}\text{Cs}$  on the interface between the contaminated rock surface and seawater. A simple dose rate estimation is carried out for two ICRU tissue substitutes placed on the interface.

**Keywords:** Fukushima Daiichi Nuclear Power Plant, Levels of  $^{137}\text{Cs}$  on rugged reefs  
Simulation of transport of 662 keV gamma rays, Scalar flux of low energy gamma rays

## Introduction

On March 11th, 2011, the Great East Japan Earthquake and subsequent tsunami crippled the Fukushima Daiichi Nuclear Power Plant (FD1NPP) of the Tokyo Electric Power Company. Consequently, a vast amount of radioactive materials were released into the atmosphere [1, 2]. Immediately after the disaster, surveys of distribution and level of contamination with  $^{134}\text{Cs}$  and  $^{137}\text{Cs}$  started on land, and the obtained results are now compiled and made available to the public by the Nuclear Regulation Authority, Japan (NRA) [3]. Regarding the contamination of the Pacific Ocean, in addition to the atmospheric fallout, heavily contaminated cooling water was directly discharged into the sea [4]. Less contaminated groundwater and river inflows have also been the sources of contamination of the ocean. An article by Buesseler et al. [5] reviewed what happened in terms of the sources, transport, and fate of Fukushima-derived radionuclides in the ocean. Surveys of the oceanic dispersion of  $^{134}\text{Cs}$  and  $^{137}\text{Cs}$  in the North Pacific and adjacent seas began immediately after the accident. A comprehensive review article on the subject is given by Kaeriyama [6].

The survey of contamination on the seafloor of the coastal ocean has remained relatively limited because of many technical difficulties. A usual sampling method can be applied only to soft seafloor. In contrast, a method that tows a gamma-ray spectrometer on the seafloor by a ship is powerful for in situ and continuous measurement, but not quite suitable for rugged reefs with meter-scale rock structures. Using the sampling method, Kusakabe et al. [7, 8], Black and Buesseler [9], and Ambe et al. [10] surveyed the distributions of  $^{137}\text{Cs}$  and some other radioactive nuclides in the sediments collected from the soft seafloor not too far from the coastline. As for in situ and continuous measurements, Thornton et al. [11, 12] developed a towed gamma-ray spectrometer. In that, a standard combination of a NaI(Tl) scintillator and a photomultiplier tube with a signal processing module was accommodated into a flexible hose to be towed by a ship. They surveyed the distribution of  $^{137}\text{Cs}$  on the seafloor of a rectangular area, from  $37^{\circ}20'$  N to  $37^{\circ}30'$  N and from  $141^{\circ}03'$  E to  $141^{\circ}15'$  E. They found high level spots of an order of  $10^4$  Bq/kg-wet. They demonstrated that the towing method has been advantageous in mapping the continuous distribution of  $^{137}\text{Cs}$  on not severely rugged seafloor.

Regarding the contamination on shallow rugged reefs lying close to the coastline where the heavily contaminated cooling water flowed through toward the sea, no detailed survey had been reported until a study by Suzuki et al. [13] (hereafter called our previous study) was published. We have shown that the levels of residual  $^{137}\text{Cs}$  ranged

from  $1 \times 10^4$  Bq/m<sup>2</sup> to  $6 \times 10^4$  Bq/m<sup>2</sup>. In the study, we established a handy means for an in situ and stationary measurement of an energy spectrum of gamma rays on flat rock surfaces in shallow reefs. According to a published geochemical survey of the area, the natural potassium, K, is evenly distributed [14]. The uniqueness of the method is that the contact between the detector and the surface of rocks is monitored by measuring the count rate of the photopeak of <sup>40</sup>K which always coexists in the measured energy spectrum. The surveyed areas are the under-water east foot of the Abukuma mountains which consist mostly of granitic rock.

It is interesting to note that the in situ gamma-ray energy spectra on the seafloor of the Irish and Kara Seas measured by Povinec et al. [15] with a submersible assembly of a high-purity Ge detector and a NaI(Tl) detector and those obtained in our previous study have a distinct feature that the count rate monotonically increases toward the low energy end of the energy spectra. However, the feature has not been addressed explicitly in either of these studies.

One aim of the present study is to give an overview of the distribution and the levels of <sup>137</sup>Cs on shallow rugged reefs obtained by extending our survey to areas untouched in our previous study with the use of a newly improved CsI(Tl) gamma-ray spectrometer. Another aim is to discuss the above-mentioned feature observed in the energy spectra of gamma rays with the use of analyses of the transport of 662 keV gamma rays near the interface between seawater and the surface of rocks in reefs.

## **Experimental**

The methodological information such as the instrumentation, characterization of the detector, and the procedure of the measurements of energy spectra of radiations on the reefs is too lengthy for this section. However, the information is indispensable for readers to understand the reliability of our method and the credibility of the data to be described below. Therefore, it is dealt with in the companion paper by Suzuki et al. [16] (hereafter called Part 2).

### **1. Area surveyed**

The area we surveyed from May 2018 to November 2019 is depicted in Fig. 1. The dates of the measurements, the GPS coordinates, and the levels of residual <sup>137</sup>Cs are listed in Table 1S in the Supplementary information. Although there is no officially certified marine chart for reefs in the area, information communicated privately from the Fukushima Prefectural Fisheries Experimental Station and advice given by the

captain of our fishing boat, Choeimaru, made it possible for us to find reefs which lie in a rectangular area between the FD1NPP and Fukushima Daini Nuclear Power Plant (FD2NPP), and between the coastline and 141.06 ° E. The reefs lie at a depth of 10 to 20 m. Even today, access to an area within a radius of 2 km from the FD1NPP is prohibited for security reasons. Beyond that, the area within a radius of 5 km is allowed to be surveyed, after notifying the Japan Coast Guard of the purpose of our survey with the GPS coordinates of the points we visit.

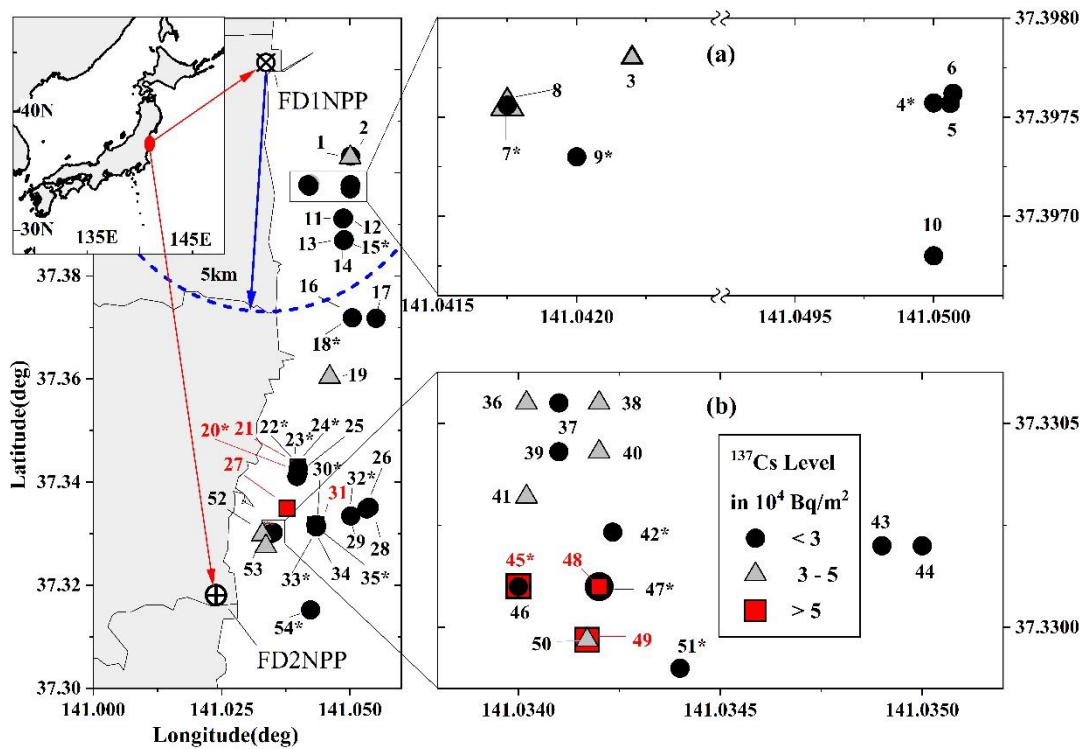


Fig. 1 Measurement points and levels of residual  $^{137}\text{Cs}$

The color and shape of the marker is a rough indication for the levels of  $^{137}\text{Cs}$  in units of  $1 \times 10^4 \text{ Bq/m}^2$ , 1 < black < 3,  $3 \leq \text{gray} < 5$ , and  $5 \leq \text{red} < 10$ . The number assigned to each point corresponds to the number in the first column of Table 1S. Two regions where the measurement points are congested are shown separately on an enlarged scale. FD1NPP indicates the location of Fukushima Daiichi Nuclear Power Plant, and FD2NPP does that of Fukushima Daini Nuclear Power Plant. The data with an asterisk are reproduced from Ref. [13].

## 2. Data Analyses and Results

A typical raw spectrum measured at Point-48 in Fig. 1 and a spectrum of background, the measurement of which is described in Part 2, are shown in Fig. 2. The rest of the measured raw spectra are depicted in Fig. 1S in the Supplementary information. In the following, “obtained spectrum” means a spectrum obtained by subtraction of the spectrum of background from the measured raw spectrum. (See Section 5. Operation in Part 2.)

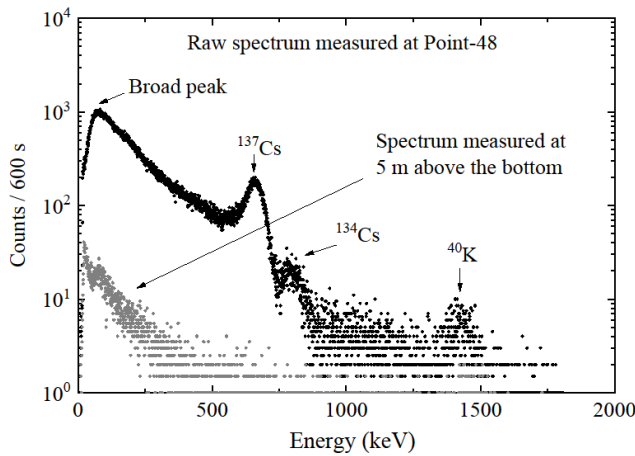


Fig. 2 Raw spectrum measured at Point-48

The upper spectrum is the raw spectrum measured at Point-48. The lower featureless spectrum is the background spectrum measured at 5 m above the bottom. The broad peak near 82 keV is defined in Section 2.2.

### 2.1 $^{40}\text{K}$ photopeak intensity

It is crucial to confirm that the detector and the flat part of the surface of the rocks are in contact configuration. As in our previous study, the confirmation was made by examination of near uniformity of intensities of the photopeak of  $^{40}\text{K}$  over all the measurement points. The obtained spectra are analyzed using Origin Pro 2018 (Origin Lab Co., Northampton, MA, USA). In the energy range between 1.2 MeV and 1.7 MeV, after a B-spline function is fitted to a baseline, a simple Gaussian function is fitted to the photopeak of  $^{40}\text{K}$ . The number of counts under the fitted Gaussian function of each obtained spectrum is plotted in Fig. 3.

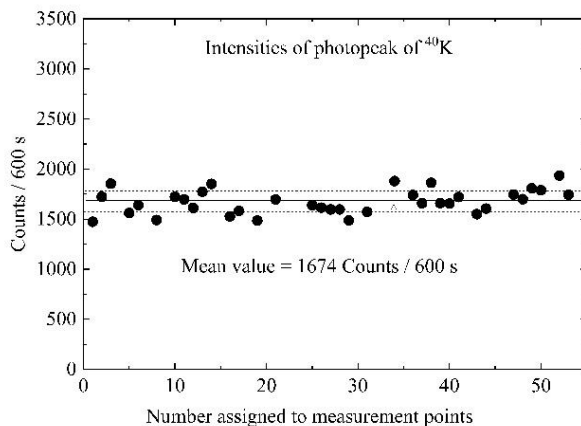


Fig. 3 Intensities of photopeak of  $^{40}\text{K}$

Number of counts under a Gaussian function fitted to the photopeak of  $^{40}\text{K}$  of each measured spectrum are plotted. The broken horizontal thin lines show  $\pm 6\%$  of the mean value.

It is shown in the Supplementary information for Part 2 that the observed mean value of 1674 counts/600 s, (2.79 counts per second) corresponds to a value expected in a case when the detector is in the contact configuration with granite rock of a thickness of about 60 mm. The count rates are distributed around the mean value with a width of  $\pm 6\%$ . The geochemical map of the area [14] shows that the natural K is distributed evenly over the area, and the concentration of  $K_2O$  is  $(1.66 \pm 0.10) \%$ . The uncertainty of evenness is considered to be the same as that in the concentration of  $K_2O$ , that is,  $\pm 6.0\%$  ( $0.10/1.66 = 6.0 \times 10^{-2}$ ). Then, the same can be said for  $^{40}K$ . The distribution of the count rates around the mean value is in reasonably good accord with the uncertainty of the evenness of the concentration of  $K_2O$ . This leads to that the contact between the detector in a pressure-tight vessel (PTV) and the flat part of the surface of the rocks is properly established. The details are described in the Supplementary information for Part 2.

## 2. 2 Levels and distribution of $^{137}Cs$

In the energy range between 490 keV and 920 keV, which covers the 605 keV photopeak of  $^{134}Cs$ , the 662 keV photopeak of  $^{137}Cs$ , and the 796 keV photopeak of  $^{134}Cs$ , first, a B-spline function is fitted to a baseline, then, three Gaussian functions of a full width at half maximum (FWHM) of 66 keV which is obtained in Part 2 are fitted to the three photopeaks. The photopeak of 609 keV from natural  $^{214}Bi$  is indistinguishable from the 605 keV peak of  $^{134}Cs$ . The levels of  $^{137}Cs$  are deduced using the count rate of the photopeak of  $^{137}Cs$  in units of counts per second (cps) and the conversion factor ( $3.29 \times 10^3$  Bq/m<sup>2</sup>/cps), the determination of which is also described in Part 2. The natural decay of  $^{137}Cs$  is only 8 % in 3.5 y which is the period of the present survey. Throughout this paper the levels are as of the measurement dates, not decay corrected.

The  $^{137}Cs$  level in units of Bq/m<sup>2</sup> at each point depicted in Fig. 1 is listed in Table 1S in the Supplementary information. The GPS coordinates and the dates of measurements are also listed in Table 1S. The numbers attached to the measurement points in Table 1S are the same as those in Fig. 1. Our previously published data measured in 2016 and 2017 are also reproduced in Fig. 1 and Table 1S with an asterisk. Since our measurement time is fixed at 600 s, the statistical uncertainty depends on the number of counts under the fitted 662 keV photopeak of  $^{137}Cs$ . It ranges from  $\pm 0.9\%$  to  $\pm 1.6\%$ . Therefore, the overall uncertainty in the levels is determined chiefly by the uncertainty in the evenness of the distribution of  $^{40}K$  over the area and in the contact configuration between the detector in the PTV and the flat part of the surface of the rocks. In the Supplementary information for Part 2 the discussion is made on these two causes of

uncertainty. It is concluded that the overall uncertainty is  $\pm 6.0\%$ , at most  $\pm 10\%$ .

Referring to Fig. 1, we notice that the distribution of residual  $^{137}\text{Cs}$  on the flat surface of the rock in the reefs is uneven over the measurement points. The levels vary from  $1.0 \times 10^4 \text{ Bq/m}^2$  to  $9.9 \times 10^4 \text{ Bq/m}^2$ . Relatively high levels are found in an area between  $37.33^\circ \text{ N}$  and  $37.34^\circ \text{ N}$ . In order to see the uneven accumulation of  $^{137}\text{Cs}$  on a much shorter scale, the points are replotted in two enlarged figures. The lower enlarged figure covers an area between  $141.0340^\circ \text{ E}$  and  $141.0350^\circ \text{ E}$ , and between  $37.3300^\circ \text{ N}$  and  $37.3305^\circ \text{ N}$ . The size of the area is about  $89 \text{ m} \times 56 \text{ m}$ . Even in this narrow area, the levels vary wildly. The records of the GPS coordinates listed in Table 1S show that the points are spaced by  $9 \text{ m}$  East-West and  $22 \text{ m}$  North-South.

All the obtained spectra have a common distinct feature: in the energy range below the photopeak of  $^{137}\text{Cs}$ , the count rate monotonically rises on a logarithmic scale with the decrease of energy to reach the highest rate around  $82 \text{ keV}$ , then starts to fall and drops sharply around  $50 \text{ keV}$  which is the very end of the effective energy range of the detector (See Part 2). On a linear scale it looks like a broad peak around  $82 \text{ keV}$ . Hereafter, this characteristic feature is called the broad peak, and the height of the broad peak means a count rate averaged over several channels in the highest parts of the peak. It should be emphasized that the broad peak is not an artifact caused by the detector and its electronic circuits. Further, a raw spectrum of  $^{137}\text{Cs}$  plate source measured in our laboratory, shown in Fig. 3 of Part 2, does not have this characteristic broad peak around  $82 \text{ keV}$ . Therefore, the presence of the broad peak suggests some underlying physical process. After examining all the obtained spectra, we note that the height of the broad peak is positively correlated with that of the photopeak of  $^{137}\text{Cs}$ . This fact strongly indicates that the characteristic feature must originate in the interaction of the  $662 \text{ keV}$  gamma rays with the rock constituents and seawater. According to the mass attenuation coefficients of gamma rays for water depicted in Radiological Health Handbook [17], the interaction of gamma rays with electrons in water molecules is mainly through the Compton (incoherent) scattering in an energy range between  $60 \text{ keV}$  and  $1 \text{ MeV}$ . Only below  $60 \text{ keV}$ , the coherent scattering and the photoelectric effect come to be involved. Therefore, the gamma rays of  $662 \text{ keV}$  emitted directly into the seawater would undergo the Compton scattering with electrons in water molecules. Similarly, those emitted into the rock would undergo the Compton scattering with electrons of rock constituents, and eventually, some of them would come back into the seawater.

The obtained spectrum consists of the pulse height distribution of radiations coming from outside the detector and the so-called Compton continuum which is inevitably created inside the detector. Therefore, to discuss a true pulse height distribution in the

region below 662 keV, we have to subtract the spectrum of the Compton continuum created by gamma rays emitted from  $^{137}\text{Cs}$  and  $^{134}\text{Cs}$  with the current ratio of  $^{134}\text{Cs}$  and  $^{137}\text{Cs}$ . The determination of the spectrum of the Compton continuum is made in Part 2.

Subtraction of the spectrum of the Compton continuum from an obtained spectrum is made by bringing the height of the photopeak of 662 keV in the spectrum of the Compton continuum to be the same as that of the obtained spectrum, as shown in Fig. 4.

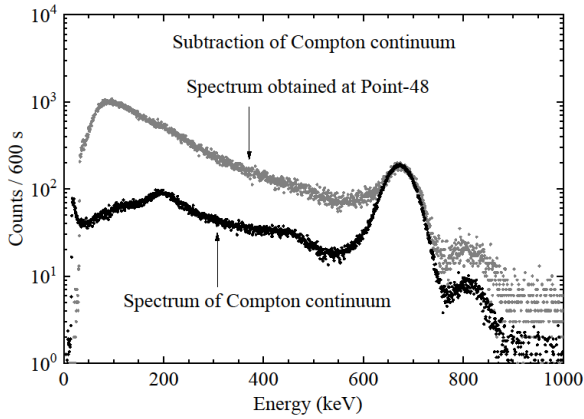


Fig. 4 Subtraction of the Compton continuum

The obtained spectrum of Point-48 and the normalized Compton continuum which is obtained empirically in Part 2 are shown.

Finally, the resultant spectrum is corrected with the energy-dependent absorption efficiency of a CsI(Tl) scintillator of a thickness of 25 mm. The efficiency used in the present calculation is obtained by digitizing the corresponding curve of Fig. 9 given by Saint-Gobain Crystals [18]. Conversion of the units of [counts/channel/600 s] to the units of scalar flux, [number of photons/cm<sup>2</sup>/s], is made using the measurement time, the area of the detector's window for gamma rays. The result for Point-48 is shown in Fig. 5. The channel width is 0.6089 keV, hereafter, rounded to 0.61 keV.

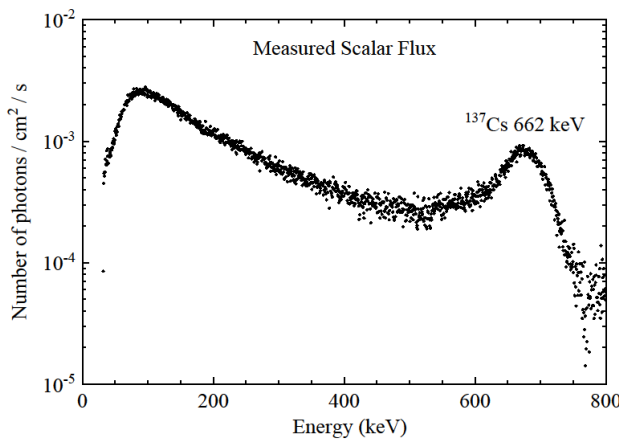


Fig. 5 Measured scalar flux

The measured scalar flux at Point-48 deduced from the obtained spectrum with the use of the detector's empirically determined Compton continuum is shown. The unit of the vertical axis is number of photons/cm<sup>2</sup>/s, where the channel width  $dE = 0.61$  keV and a source strength is  $9.9 \times 10^4$  Bq/m<sup>2</sup>.

## Transport of 662 keV gamma rays

Many studies of the transport of the 662 keV gamma rays in water, and other soft and hard materials have been reported. To the best of the authors' knowledge, however, no study has aimed to specifically examine the transport of the 662 keV gamma rays on both sides of the interface between contaminated rock surface and seawater. Here, we set a simple model of a water-filled pool to analyze the transport of the 662 keV gamma rays on both sides of the interface using Monte Carlo N-Particle Transport Code (MCNP Transport code) produced by Los Alamos National Laboratory [19].

The water-filled pool has a depth of 2 m with a bottom set to ordinary concrete with a density  $\rho$  of  $2.3 \text{ g/cm}^3$  (for composition, see Ref. [20]). A cell of a cylinder, the radius of which is 0.5 m, is set on the bottom. A circular plane source of 0.5 m radius and a unit amount of  $^{137}\text{Cs}$  is placed at the bottom of the cell. A reflecting boundary condition is set on the surface of the cylindrical cell to simulate an infinitely extended source and floor. A sphere-shaped volume tally of 0.10m diameter is placed on the center of the bottom of the cell. The volume tally called F4 in the manual of the MCNP Transport code gives an energy spectrum of angle-integrated flux in units of [number of photons/cm<sup>2</sup>/s], where the channel width  $dE$  is 0.35663 keV in the present calculation. Hereafter, it is rounded to 0.36 keV. From now on, following the manual, the angle-integrated flux is called the scalar flux. The volume tally called F6 in the manual gives a spectrum of energies deposited to the medium in the tally (in the present study, the medium is water) in units of energy  $\times$  number of photons/cm<sup>2</sup>/s. As for photon interactions, the detailed physics treatment, which includes incoherent (Compton) scattering, photoelectric absorption, and coherent (Thomson) scattering, is employed. The number of trials is  $2 \times 10^8$ . As for precision, the fractional standard deviation at 662 keV is 0.0011, and that at other energies is 0.01-0.04. This good conversion result is attained without applying any variance-reduction technique.

Figure 6 shows the result of the simulation of the scalar flux in the F4 tally as a function of energy for the water-filled pool. There are two prominent structures; one is a high and very narrow peak with a width of just one channel (0.36 keV) at 662 keV, and the other is the step at 184.4 keV. Another feature is that the scalar flux monotonically rises to make a broad peak with a decrease in energy until it starts to drop at around 50 keV. Qualitative explanations for these features are as follows. First, the gamma rays of 662 keV are emitted into the concrete bottom from a point where the tally contacts the bottom. After being backscattered with a scattering angle of  $\pi$ , the gamma rays of 184.4 keV come back on the same path and hit the tally. The mean free path of the 184.4 keV

gamma rays in water is about 0.05 m. It is the same as the tally's radius. This means that the incoming 184.4 keV gamma rays probably interact at least once with water inside the tally. Then, the tally registers the incoming gamma ray of 184.4 keV and the outgoing gamma ray of other energy below 184.4 keV. In addition, the gamma rays emitted into the concrete bottom are scattered multiple times with various scattering angles, and some of them eventually surface back to the interface and behave as if an additional source with a continuous energy spectrum. As a result, the scalar flux of low energy gamma rays increases. When the gamma rays of 662 keV are emitted into the water, a very similar picture can be imagined as in the case of the concrete bottom, even though the density of water is lower than that of the concrete. After being backscattered with a scattering angle of  $\pi$ , the gamma rays of 184.4 keV come back on the same path and hit the tally. Some of the gamma rays come back after being scattered multiple times somewhere above the tally, and they act as an additional source with a continuous energy spectrum. Consequently, the broad peak is formed around 50 keV in the spectrum of the scalar flux.

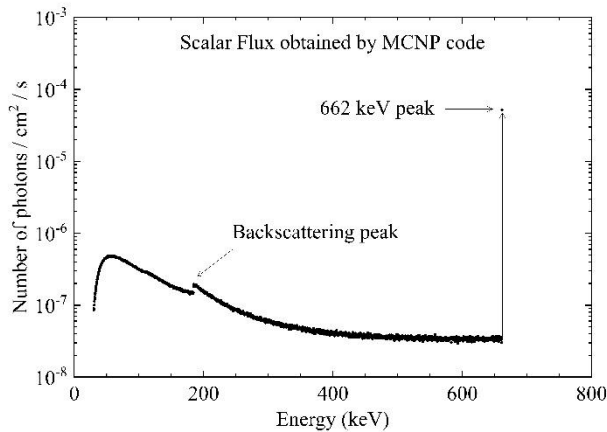


Fig. 6 Scalar flux obtained by MCNP transport code

The energy spectrum of the scalar flux in the F4 tally placed on the bottom of the water-filled pool is obtained by Monte Carlo N-Particle Transport Code, Ver. 4B by Los Alamos National Laboratory. The channel width  $dE$  is 0.36 keV.

## Discussion

### 1 Levels of residual <sup>137</sup>Cs

We keep in mind that comparing the present results with those published earlier is made with no decay correction because the half-life of <sup>137</sup>Cs is 30.1 y, and a few years of difference in the measurement dates make a difference of only several percent of the measured levels. The present results on the shallow rugged reefs are consistent with those reported in our previous survey which showed that the levels of residual <sup>137</sup>Cs on

the flat part of the surface of the rocks in the reefs were in order of  $10^4$  Bq/m<sup>2</sup>. Comparison with the previously reported levels for soft seafloor areas, which lie farther east from the coastline, is not so straightforward. In the present study, the level of <sup>137</sup>Cs is in units of Bq/m<sup>2</sup> because we have assumed that the residual <sup>137</sup>Cs on the rock surface is two-dimensionally extended with practically no vertical distribution. On the other hand, it is now well known that tiny particles of several types of phyllosilicate accommodate <sup>137</sup>Cs in them and settle at the bottom, then penetrate downward by various mechanisms into the soft seafloor. The profile of a vertical distribution depends on the constituents of the soft seafloor. Therefore, the data obtained by the sampling method are usually presented in units of Bq/kg, and a direct comparison of the present results with those obtained in the soft seafloor areas is not always possible.

Four reports are available for the purpose of comparison. One report is published by The National Maritime Research Institute [21]. They towed their detector to continuously measure the levels along a survey line of about 37 km in length, which lay between 37.18° N to 37.52° N and approximately 3 km away from the coastline. The depth varied from 15 m to 23 m. The survey line ran due east of our surveyed area by about 2 km. In parallel with towing the detector, they sampled sediments at eight points on the survey line to obtain vertical profiles of <sup>137</sup>Cs accumulation. The vertical profiles made it possible to change a value in units of Bq/kg to that in Bq/m<sup>2</sup>. There was a high-level spot of  $1.1 \times 10^5$  Bq/m<sup>2</sup> southeast of the FD1NPP, and another one was  $4.0 \times 10^4$  Bq/m<sup>2</sup> east of the FD2NPP. In the area between the two spots, the level varied from  $0.2 \times 10^4$  Bq/m<sup>2</sup> to  $2.0 \times 10^4$  Bq/m<sup>2</sup>. The comparison of these data with the present results indicates that the <sup>137</sup>Cs levels on the shallow rugged reefs are not much different from those on the soft seafloor, which extends eastward from the reefs.

The second data are found in a report by Kusakabe et al. [8]. Since 2011, they have systematically monitored <sup>137</sup>Cs on the seafloor using the sampling method in a wide area on the continental shelf off Fukushima. Among their monitoring stations, the closest to the present survey is E1(37.417° N, 141.373° E) which is located 30 km due east of the FD1NPP, and the depth is about 135m. The sediment type is sand-silt-clay. The level at E1 deduced from their Fig. 11 by the present authors is  $1.4 \times 10^4$  Bq/m<sup>2</sup> in November 2014,  $2.6 \times 10^4$  Bq/m<sup>2</sup> in May 2015, and  $3.2 \times 10^4$  Bq/m<sup>2</sup> in November 2015. They are in the same order of magnitude as that of our present and previous results on No. 1 to No. 9 obtained in 2017-2019, as shown in Table 1S.

The third data, which can be used for not exactly direct but semi-direct comparison, can be found in a report by Otosaka et al. [22]. Using the sampling method, they reported the levels of <sup>137</sup>Cs in seawater, seabed sediment, and pore water collected

between 2015 and 2018. Among their 16 monitoring stations, the station NP0 (37.417° N, 141.050° E) is the closest to the present survey. They found that the level was 145.5 Bq/kg in November 2016, 146.4 Bq/kg in September 2017, and 88.8 Bq/kg in September 2018. Although they did not provide the relevant vertical profiles, from the given density of 1.29 g/cm<sup>3</sup> and the length of the sampled core of 10 cm, it is possible to approximately change their values in units of Bq/kg to the inventory in units of Bq/m<sup>2</sup>. The conversion made by the present authors yielded that the levels were 1.9×10<sup>4</sup> Bq/m<sup>2</sup> in November 2016 and in September 2017, and 1.1×10<sup>4</sup> Bq/m<sup>2</sup> in September 2018. These levels are similar to or slightly lower than those we obtained at our points No. 1, 2, 5, and 6 measured during the period from 2018 to 2019.

The fourth data are found in a report published by Nuclear Regulation Authority, Japan [23]. They covered an area between the coastline and 141°30'E, and 37°10'N and 37°40'N by the sampling method. The sediment type is silt. Several points lie close to our measurement points. The levels at these points vary from 4.61×10<sup>4</sup> Bq/m<sup>2</sup> to 37.08×10<sup>4</sup> Bq/m<sup>2</sup>. Some of them are higher by an order of magnitude than those we found on the reefs.

From the above comparison, we conclude that, although the reefs we surveyed were once the path for the highly contaminated water to go into the ocean, the levels on reefs are similar to or lower than those reported on the soft seafloor of the continental shelf off Fukushima. Regarding the distribution of <sup>137</sup>Cs, Thornton et al. [12] and Black and Buesseler [9] reported that the distribution was strongly influenced by meter-scale features of the seafloor terrain. From the enlarged figure (b) of Fig. 1, the same can be said to the shallow rugged reefs with meter-scale rock structures.

## **2 Scalar flux of radiations**

Regarding the results of the MCNP simulation, it should be noted that the simulation does not include the presence of the PTV, the detector and its casing. Therefore, a quantitative comparison cannot be made with the measured spectrum. Nevertheless, a qualitative comparison between the simulated and the measured spectrum is informative. For that purpose, the simulated results are normalized to the observed source strength of 9.9×10<sup>4</sup> Bq/m<sup>2</sup> at Point-48. While the energy resolution function of the simulation is a rectangular function of a width of 0.36 keV, the energy resolution of the measurement can be represented by a single Gaussian function. However, the FWHM is energy-dependent, 66 keV at 662 keV and 16.7 keV at 59.5 keV as described in Part 2. Therefore, it is unwise to guess an analytical form of the energy resolution from these two data. Instead, we demonstrate the effects of convolution in two representative cases,

one is a Gaussian function of the FWHM of 66 keV, and the other is that of the FWHM of 20 keV. The results are shown in Fig. 7.

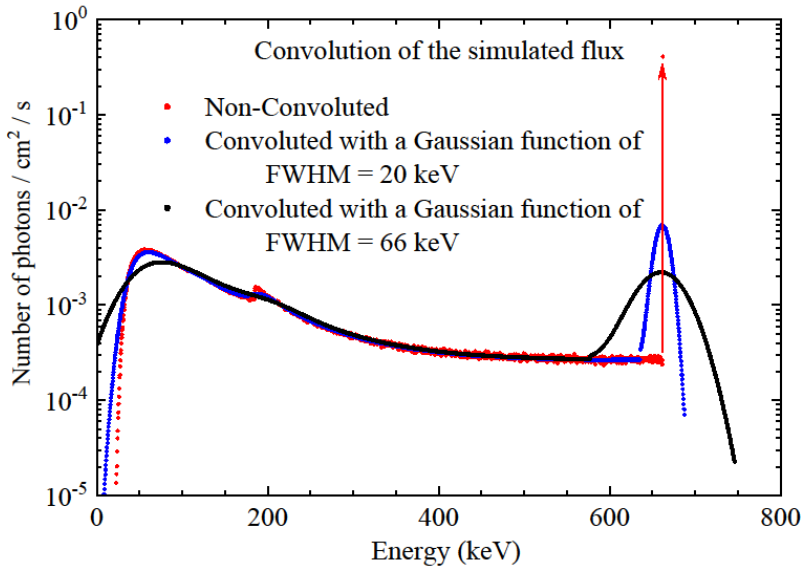


Fig. 7 Convolution of the simulated scalar flux

The red spectrum is the scalar flux for the water-filled pool shown in Fig. 6. The blue spectrum is the one convolved with a single Gaussian function of the FWHM = 20 keV. The black spectrum is the one convolved with a single Gaussian function of the FWHM = 66 keV.

In the case of the FWHM of 20 keV, the sharp peak at 662 keV is broadened accordingly, and the prominent structure at 184 keV is smeared, but the broad peak around 50 keV is less affected. In the case of the FWHM of 66 keV, the 662 keV peak is broadened further, the structure at 184 keV becomes hardly recognizable, and the broad peak around 50 keV becomes dulled and shifted to near 80 keV. However, both cases do not strongly affect the shape of the spectrum in the energy region between 200 keV and 550 keV. Therefore, the convolution with a Gaussian function of the FWHM of 66 keV is an acceptable approximation for the qualitative comparison between simulation and measurement.

In order to present the simulated spectrum with a channel width of 0.36 keV and the measured one with that of 0.61 keV in one figure, five channels are binned for the simulated spectrum and three channels are binned for the measured spectrum to make the channel width nearly the same to each other. The height of both fluxes at each energy point is increased accordingly. The results are shown in Fig. 8.

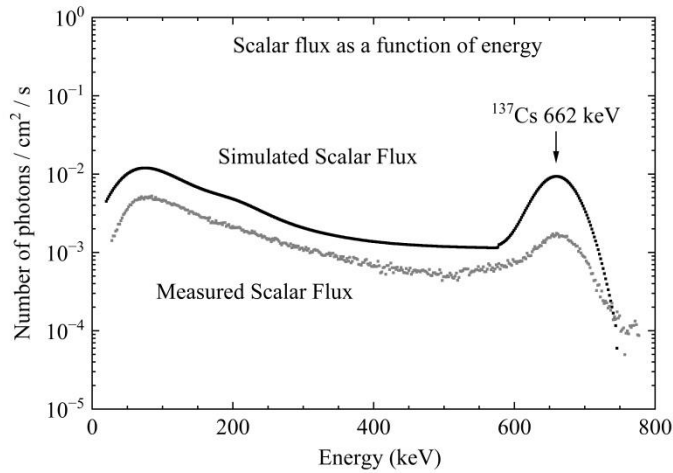


Fig. 8 Comparison between the measured flux and the simulated flux

The black spectrum is the simulated flux convoluted with a single Gaussian function of the FWHM = 66 keV. The gray spectrum is the measured flux. The source strength for both spectra is  $9.9 \times 10^4$  Bq/m<sup>2</sup>.

The simulated scalar flux has reproduced the characteristic features of the measured one well. The multiple Compton scattering of the 662 keV gamma rays from <sup>137</sup>Cs on the interface between seawater and seafloor is the cause of the monotonic rise of the scalar flux toward the low energy end with the broad peak around 82 keV.

Regarding the non-convoluted scalar flux in Fig. 7, when the scalar flux is summed over the energy range below 662 keV, the sum is 2.7 times larger than the flux only at 662 keV. The mass energy-absorption coefficients,  $\mu_{en}(E)$ , of tissue substitutes in ICRU Report 44 [24] increase exponentially with the decrease of energy in the energy region below 80 keV. Thus, the low energy gamma rays should not be disregarded in estimating the chronic external exposure of benthic organisms from the residual <sup>137</sup>Cs on the seafloor. Once the scalar flux and  $\mu_{en}(E)$  for a target medium are given as a function of energy (e.g., Hubbell and Seltzer [25]), we can estimate the amount of energy absorbed by the medium placed on the bottom. In the Supplementary information, the calculation process is described. In the case of source strength of  $1 \times 10^5$  Bq/m<sup>2</sup>, the highest level found in the present survey, we obtain 0.11  $\mu$ Gy/h for the tissue substitute ICRU-44 Cortical bone ( $\rho = 1.92$  g/cm<sup>3</sup>), and 0.085  $\mu$ Gy/h for the tissue substitute ICRU-44 Skeletal muscle ( $\rho = 1.05$  g/cm<sup>3</sup>).

## Conclusions

Measurements of gamma-ray spectra with the use of the in situ and stationary method on the shallow reefs lying inshore of Fukushima from December 2017 to July 2019 have revealed that the levels of residual <sup>137</sup>Cs vary from  $1.0 \times 10^4$  Bq/m<sup>2</sup> to  $9.9 \times 10^4$

Bq/m<sup>2</sup>. The levels are similar to those reported on the soft seafloor of the continental shelf next to the reefs. The distribution is strongly influenced by the meter-scale rock structures. The gamma-ray spectra have revealed a high flux of gamma rays of energies less than 662 keV. The Monte Carlo simulation on the simplest model of a water-filled pool has shown that the multiple Compton scattering of the 662 keV gamma rays on both sides of the interface between the surface of rocks and seawater causes the rise of the flux of low energy gamma rays. The high flux of low energy gamma rays should be considered in estimating chronic external exposure of benthic organisms from residual <sup>137</sup>Cs on the bottom of the sea.

## Acknowledgments

The authors thank Iwaki Fishery Cooperative and Futaba-Soma Fishery Cooperative for understanding the aim of our survey and for introducing us to Captain Ishii and his fishing boat Choeimaru. We greatly appreciate Captain Hirokazu Ishii's knowledge of the reefs and his skill in keeping his boat at a designated point against winds and currents. We are grateful to the Institute for Cosmic Ray Research, the University of Tokyo for letting us use the radiation detection module C12137-10. Precious suggestions from H. Akai in preparing of the manuscript are gratefully acknowledged. Without generous supports from M. Imazeki, J. Yamada, N. Kumagai, Y. Yamada, K. Sato, H. Tejima, H. Kurahayashi, W. Takahashi, T. Takaishi, S. Itou, K. Itou, A. Okada, E. Shinoda, K. Kinoshita, Y. Sato, M. Tsuchida, technical staff members of LightStone Corp., the late H. Fujibayashi and the late Y. Okuizumi, this research project would not have been carried out.

## Supplementary information

1. Table 1S: Dates of measurements, GPS coordinates, and levels of <sup>137</sup>Cs.
2. Fig. 1S: All the measured spectra.
3. A simple estimation of dose rate.

## References

1. Gov. Jpn. (2011) Report of the Japanese Government to the IAEA Ministerial Conference on Nuclear Safety - The Accident at TEPCO's Fukushima Nuclear Power Stations - June 2011.  
[http://japan.kantei.go.jp/kan/topics/201106/iaea\\_houkokusho\\_e.html](http://japan.kantei.go.jp/kan/topics/201106/iaea_houkokusho_e.html) (Accessed

Jan. 3, 2024).

2. IAEA (International Atomic Energy Agency) (2011) Mission report. The Great East Japan Earthquake Expert Mission. In: IAEA International Fact Finding Expert Mission of the Fukushima Dai-ichi NPP Accident Following the Great East Japan Earthquake and Tsunami, pp. 1-160. [EBO \(iaea.org\)](http://www.iaea.org) (Accessed Jan. 3, 2024).
3. Nuclear Regulation Authority, Japan (2021) <http://radioactivity.nra.go.jp/en/> (Accessed Jan. 3, 2024).
4. Tsumune D, Tsubono T, Aoyama M, Hirose K (2012) Distribution of oceanic  $^{137}\text{Cs}$  from the Fukushima Dai-ichi Nuclear Power Plant simulated numerically by a regional ocean model. *J. Environ. Radioact.* 111:100-108.
5. Buesseler K, Dai M, Aoyama M, Benitez-Nelson C, Charmasson S, Higley K, Maderich V, Masqué P, Morris P J, Oughton D, Smith J N (2017) Fukushima Daiichi-Derived Radionuclides in the Ocean: Transport, Fate, and Impacts. *Annu. Rev. Mar. Sci.* 9: 173-203.
6. Kaeriyama H (2017) Oceanic dispersion of Fukushima-derived radioactive cesium: a review. *Fish. Oceanogr.* 26: 99-113.
7. Kusakabe M, Oikawa S, Takata H, Misonoo J (2013) Spatiotemporal distributions of Fukushima-derived radionuclides in nearby marine surface sediments. *Biogeosciences* 10: 5019-5030.
8. Kusakabe M, Inatomi N, Takata H, Ikenoue T (2017) Decline in radiocesium in seafloor sediments off Fukushima and nearby prefectures. *J. Oceanogr.* 73: 529-545.
9. Black E E, Buesseler, K O (2014) Spatial variability and the fate of cesium in coastal sediments near Fukushima, Japan. *Biogeosciences*, 11: 5123-5137.
10. Ambe D, Kaeriyama H, Shigenobu Y, Fujimoto K, Ono T, Sawada H, Saito H, Miki S, Setou T, Morita T, Watanabe T (2014) Five-minute resolved spatial distribution of radiocesium in sea sediment derived from the Fukushima Dai-ichi Nuclear Power Plant. *J. Environ. Radioact.* 138: 264-275.

11. Thornton B, Ohnishi S, Ura T, Odano N, Fujita T (2013) Continuous measurement of radionuclide distribution off Fukushima using a towed sea-bed gamma-ray spectrometer. *Deep-Sea Res. I* 79: 10-19.
12. Thornton B, Ohnishi S, Ura T, Odano N, Sasaki S, Fujita T, Watanabe T, Nakata K, Ono T, Ambe D (2013) Distribution of local  $^{137}\text{Cs}$  anomalies on the seafloor near the Fukushima Dai-ichi Nuclear Power Plant. *Mar. Pollut. Bull.* 74: 344-350.
13. Suzuki F, Ohashi H, Shibata H, Nogami K, Arakawa H, Shiotani N (2019) A trial of in situ and static measurements of levels of radioactive cesium 137 on shallow rugged reefs lying close to the coastline of Fukushima. *Mar. Pollut. Bull.* 145: 649-655.
14. Geological Survey of Japan (2003).  
<https://gbank.gsj.jp/geochemmap/ocean/chiho/Tohoku/gazou/TohokuK.gif>  
(Accessed Jan. 3, 2024).
15. Povinec P P, Osvath I, Baxter M S (1996) Underwater Gamma-spectrometry with HPGe and NaI(Tl) Detectors. *Appl. Radiat. Isot.* 47:1127-1133.
16. Suzuki F, Imazeki M, Yamada J, Yamada Y, Kumagai N, Ohashi H, Shiotani N (2024) On residual  $^{137}\text{Cs}$  on shallow rugged reefs lying inshore of Fukushima: Part 2: Methodological improvements.
17. Radiological Health Handbook (1970) U.S. Dept. Health, Education and Welfare, Rockville, MD, USA.
18. Efficiency Calculations for Selected Scintillators.  
[https://vepp2k.inp.nsk.su/~inest/halometer/SGC\\_Efficiency\\_Calculations.pdf](https://vepp2k.inp.nsk.su/~inest/halometer/SGC_Efficiency_Calculations.pdf)  
(Accessed Jan. 3, 2024).
19. Los Alamos National Laboratory (2003) LA-UR-03-1987 MCNP-A General Monte Carlo N-Particle Transport Code, MCNP Version 5, Volume I: Overview and Theory.

20. Koyama K, Okumura Y, Furuta K, Miyasaka S (1977) Multi-group Cross Section Sets for Shield Materials. JAERI-M 6928 (in Japanese), p. 36, Table C.1.  
<https://jopss.jaea.go.jp/pdfdata/JAERI-M-6928.pdf> (Accessed Jan. 3, 2024).
21. National Maritime Research Institute (2016), (in Japanese).  
<https://radioactivity.nra.go.jp/ja/contents/13000/12079/view.html> (Accessed Jan. 4, 2024).  
The report in pdf can be downloaded by clicking “part 1”.  
The report is written in Japanese. However, the parts relevant to the present discussion are Fig. 3-35 in p. 62, Fig. 3-36 in p. 63, and Fig. 3-39 in p. 66 which may be understandable to most of the readers.
22. Otsuka S, Kambayashi S, Fukuda M, Tsuruta T, Misonou T, Suzuki T, Aono T (2020) Behavior of Radiocesium in Sediments in Fukushima Coastal Waters: Verification of Desorption Potential through Pore Water. Environ. Sci. Technol. 54: 13778-13785.
23. Nuclear Regulation Authority, Japan (2020), (in Japanese).  
<http://radioactivity.nra.go.jp/ja/contents/16000/15193/view.html> (Accessed Jan. 4, 2024)
24. ICRU 44 (1989) Tissue Substitutes in Radiation Dosimetry and Measurement. J. ICRU Vol. 23(1).
25. Hubbell J H, Seltzer S M (1995) Tables of X-ray Mass Attenuation Coefficients and Mass Energy-Absorption Coefficients 1 keV to 20 MeV for Elements Z = 1 to 92 and 48 Additional Substances of Dosimetric Interest. NISTIR 5632. Natl. Inst. Standards Technol., USA.  
<https://www.nist.gov/pml/x-ray-mass-attenuation-coefficients> (Accessed Jan. 4, 2024).

### **E-mail addresses**

suzuki@ecostudies.jp (F. Suzuki), ohashi@ecostudies.jp (H. Ohashi),  
nogami@ecostudies.jp (K. Nogami), shibata@ecostudies.jp (H. Shibata),  
arakawa@kaiyodai.ac.jp (H. Arakawa),

kumeda@tohtech.ac.jp (K. Umeda), colsys-u8-kt-979@mve.biglobe.ne.jp (T. Kobayasi), shiotani@ecostudies.jp (N. Shiotani)

### **Author contributions**

Conceptualization: F. Suzuki, H. Arakawa, N. Shiotani.

Data collection and analysis: F. Suzuki, N. Shiotani, H. Ohashi, K. Nogami, H. Shibata.

Computational analysis: T. Kobayasi, K. Umeda.

Writing original draft: F. Suzuki, T. Kobayasi, N. Shiotani.

All authors discussed the results and read critically the draft.

Supervision: N. Shiotani.

*This article has not been published previously or submitted to any other journal.*

*There is no overlap with previously published works.*

*This research did not receive any specific grant from funding agencies in the public, commercial, or not-for-profit sectors.*

*Competing interests: The authors declare that they have no known competing financial interests or personal relationships that could have appeared to influence the work reported in this paper.*